MATERIALS SCIENCE

Solution-shearing of dielectric polymer with high thermal conductivity and electric insulation

Zheng Li[1], Lu An[1], Saurabh Khuje[1], Jingye Tan[1], Yong Hu[1], Yulong Huang[1], Donald Petit[1], Danial Faghihi[1], Jian Yu[2], Shenqiang Ren[1,3,4]*

Polymer dielectrics, an insulating material ubiquitous in electrical power systems, must be ultralight, mechanically and dielectrically strong, and very thermally conductive. However, electric and thermal transport parameters are intercorrelated in a way that works against the occurrence of thermally conductive polymer electric insulators. Here, we describe how solution gel-shearing–strained polyethylene yields an electric insulating material with an outstanding in-plane thermal conductivity of 10.74 W m^{-1} K^{-1} and an average dielectric constant of 4.1. The dielectric constant and loss of such sheared polymer electric insulators are nearly independent of the frequency and a wide temperature range. The gel-shearing aligns ultrahigh–molecular weight polymer crystalline chains for the formation of separated and aligned nanoscale fibrous arrays. Together with lattice strains and the presence of boron nitride nanosheets, the dielectric polymer shows high current density carrying and high operating temperature, which is attributed to greatly enhanced heat conduction.

INTRODUCTION

Dielectric polymers can operate at a high breakdown voltage used as electrical insulator material in contemporary high-power electric systems and advanced electronics (*1*–*4*). However, the miniaturization and resistive power loss in power electronic systems, producing an average heat flux of 1000 up to 5000 W/cm^2, is the absolute dominant energy loss (*5*). If this large heat flux cannot be dissipated instantly, the accumulated heat would lead to the temperature rise and cause the loss of dielectric performance gradually in polymer dielectrics, which require high operating temperatures and high breakdown conditions. The thermal conductivity of a typical polymer insulation material, such as Kapton polyimide, is around 0.17 W m^{-1} K^{-1}, inherently thermal insulating to conduct heat (*6*). Such poor thermal properties of these materials limit heat rejection, thus limiting the achievable power density and efficiency. Therefore, a principal bottleneck in high–energy density power electronics can be polymer dielectric insulation material. An electrical insulating performance measured by high dielectric constant and dielectric strength, as well as high thermal conductivity, has proved to be difficult since the electric and thermal transport parameters, i.e., σ and κ, are intercorrelated in a way via the Wiedemann-Franz law. The polymer insulators consisting of a cluster of discrete chains by weak intermolecular forces show a high resistance to heat transfer (phonons) with a negligible electronic contribution, which works against the occurrence of thermally conductive electric insulator (*7*). Advanced insulation materials should also mitigate large voltage stress (dV/dt) (*8*). The traditional method of using thicker insulation materials to accommodate the higher voltages required for substantial system efficiency is very unlikely to meet the technical metrics because of the thermal and weight concerns. Therefore, a high dielectric constant, a low dielectric loss, and a consistently high breakdown strength of thermally conductive polymer insulators are indispensable for high-power density electronics subjected to high voltages.

One of the nonmetallic thermal conductors is single-crystal diamond having thermal conductivity of 2190 W m^{-1} K^{-1}, which is attributed to its exceptionally efficient heat transmission through the lattice vibrations (*9*). This suggests a polymer material virtually "free" of crystalline defects, where its backbone chains are macroscopically aligned to enable ultrahigh thermal conductivity. This concept was first proposed in 1977 by Gibson *et al.* (*10*) on the linear nonpolar polyethylene with its repetition of —CH_2 units and virtually no branching. The demonstration was confirmed by drawing ultrahigh–molecular weight polyethylene (UHMWPE) fibers with a remarkable high thermal conductivity of 104 W m^{-1} K^{-1}, higher than metals such as platinum, iron, and nickel (*11*, *12*). However, an emerging UHMWPE electric insulator is dependent on many factors: the polymer crystallinity, the crystallite orientation, and the chain length and its molecular packing (*13*–*16*). To become an enabling thermally conductive electric insulator material, the dilemma of polyethylene is that such a symmetrical molecule is truly covalent with a low dielectric constant (*17*, *18*). In this case, it is essential to develop a new strategy to achieve high thermal conductive electric insulator polyethylene with high dielectric constant and strength (*19*–*21*). Here, we solution-gel sheared UHMWPE (SUPE) to prepare the strained flexible sheets and coatings (Fig. 1A). The markedly improved dielectric properties and thermal conductivities are ascribed to the alignment and close packing of ultrahigh–molecular weight crystalline chains, facilitating the formation of a large number of separated nanocapacitor arrays (high k and high resistivity). To our knowledge, the gel-shearing induced SUPE transparent thin films to have the outstanding thermal conductivity of 10.74 W m^{-1} K^{-1} (20 times higher than nonstrained polyethylene) and an average dielectric constant of 4.1 (1.8 times higher than nonstrained polyethylene) compared with the standard polymer dielectrics (Fig. 1B) (*22*–*25*).

RESULTS AND DISCUSSION

In the solution gel-shearing process, a shearing rod drags the solution gel across a heated substrate while driving the gel solution between

[1]Department of Mechanical and Aerospace Engineering, University at Buffalo, The State University of New York, Buffalo, NY 14260, USA. [2]Army Research Laboratory, Aberdeen Proving Ground, MD 21005, USA. [3]Department of Chemistry, University at Buffalo, The State University of New York, Buffalo, NY 14260, USA. [4]Research and Education in Energy, Environment and Water (RENEW), University at Buffalo, The State University of New York, Buffalo, NY 14260, USA.
*Corresponding author. Email: shenren@buffalo.edu

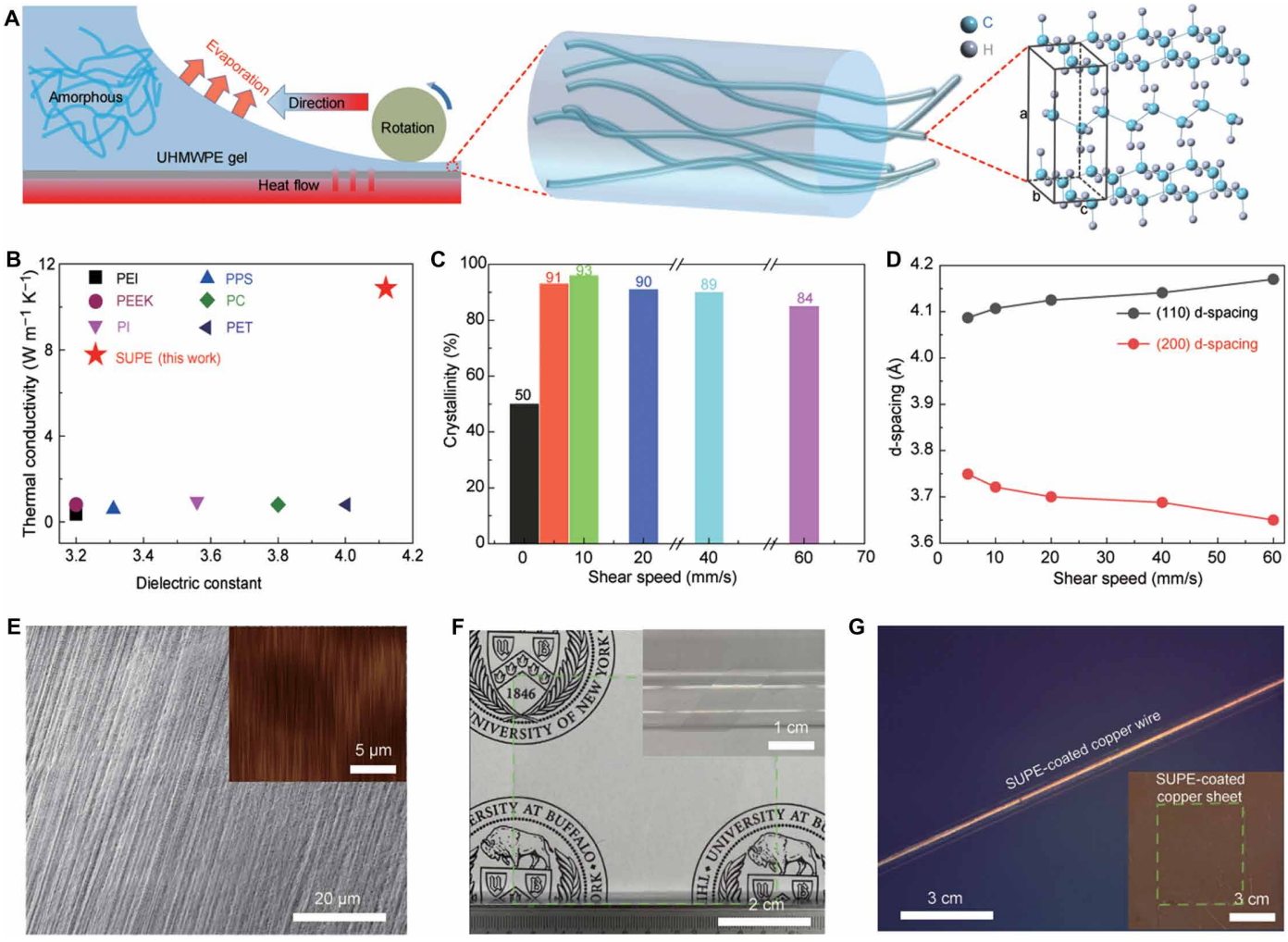

Fig. 1. Solution gel-shearing induced SUPE films with the chain alignment microstructure. (**A**) Scheme of solution gel-shearing process and chain alignment in SUPE film. (**B**) Comparisons of the thermal conductivity versus dielectric constants for this work and typical polymer dielectric and insulation materials. (**C**) Crystallinity versus shearing speeds of SUPE films. (**D**) The d-spacing changes for shearing speed–dependent SUPE films, indicating the lattice strain presence. (**E**) Scanning electron microscopy image showing a highly aligned fibrous structure induced under shearing speed of 10 mm/s. The corresponding atomic force microscopy image shows the nanofibrous alignment induced by shearing. (**F**) Flexible and transparent SUPE films. (**G**) Demonstration of transparent flexible solution sheared UHMWPE coatings for copper wires and copper foils for thermal conductive power infrastructures. Photo credit: Zheng Li, University at Buffalo.

the rod and the substrate at a controlled speed ranging from 5 to 60 mm/s together with the solvent evaporation (Fig. 1A and fig. S1) (*26*, *27*). Figure 1A illustrates the texture of transparent SUPE thin films as a function of shearing speed. In addition to altering SUPE thin film texture and domain sizes, gel-shearing speed also plays an important role in the molecular packing (crystallinity) and strain in the thin film. X-ray diffraction experiments are performed to characterize the shearing-dependent crystallinity and lattice strain (Fig. 1, C and D). A crystallinity of 93% can be achieved with a shearing speed of 10 mm/s at which the ultrahigh–molecular weight chains could be unfolded and aligned to a larger extent. As the shearing speed increases, the (110) d-spacing increases by 1.7% incrementally from 4.09 to 4.16 Å, and concurrently, the (200) d-spacing decreases by 2.4% from 3.74 to 3.65 Å (Fig. 1D). These d-spacing changes only occur for in-plane lattice parameters, while the vertical spacing does not change with shearing speed. In addition, peak broadening is observed as the gel-shearing speed increases, which is consistent with the smaller crystallite or domain sizes resulting from the rapid drying at a high shearing speed. To our knowledge, the lattice strain in SUPE thin films has not been reported in the film preparation. For a shearing speed of 10 mm/s (Fig. 1E), the oriented nanofibrous array domains with lengths of up to centimeters are observed with the long axis parallel to the shearing direction, while the fabricated SUPE films are highly flexible and transparent (Fig. 1F). This trend in SUPE shearing morphology can be observed as the electrical insulation coatings for metallic wires and substrates in thermal conductive power delivery infrastructures (Fig. 1G).

We measure the alignment effect on the dielectric performance of flexible sheared SUPE thin films. The dielectric constant and dissipation factor is measured as a function of frequency and temperature (Fig. 2). As shearing speed increases (Fig. 2A), the dielectric constant increases to a maximum of 4.6 for SUPE thin films prepared at a shearing speed of 20 mm/s. The dielectric constant decreases for faster shearing speeds to a value of 4.2 for SUPE prepared

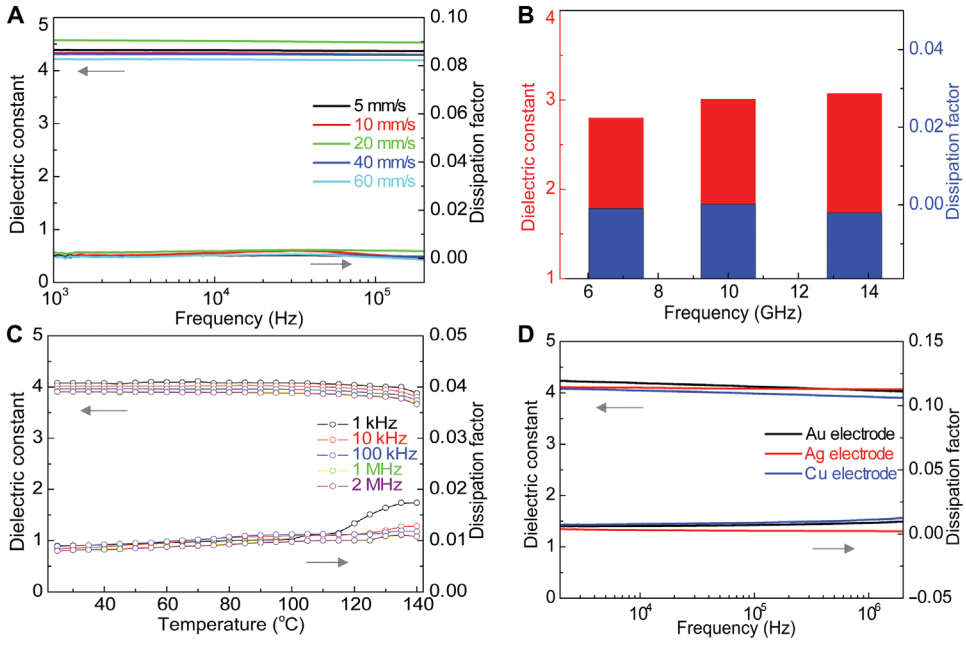

Fig. 2. Dielectric property and dielectric stability of shearing SUPE films. (**A**) Frequency dependence of the dielectric constants and dissipation factor for SUPE films under different shearing speeds. (**B**) Gigahertz frequency dependence of dielectric constant and dissipation factor of SUPE films. (**C**) Temperature dependence of dielectric constants and dissipation factor of SUPE films under various frequencies from 1 kHz to 2 MHz. (**D**) Electrode-dependent dielectric constant and dissipation factor for the SUPE films.

at a speed of 60 mm/s. We attribute the decrease in the dielectric performance observed at shearing speeds above 20 mm/s to the decrease in its crystallite domain and alignment (Fig. 1), causing an increase in the grain boundaries for weaker electronic overlapping of the ultrahigh–molecular weight chains. These dielectric films are also stable for ultrahigh frequency in gigahertz ranges (Fig. 2B); in addition, the sheared SUPE offers the stable dielectric constant and dissipation factor in the frequency range of 10^3 to 10^6 Hz at high temperatures (Fig. 2C), while no relaxation of electronic dipoles is observed at high temperatures. We attribute our higher dielectric performance of SUPE films to the improved electronic coupling between aligned ultrahigh–molecular weight chains in the strained films (*1*). This conclusion is further supported by the observation that high dielectric performance is observed for different electrode contacted films while maintaining the same textures and crystallinity. The results of electrode-dependent dielectric constant and dissipation factor for the SUPE films indicated that the electrode hardly affects the dielectric of the SUPE films (Fig. 2D).

The shearing speeds play an important role in controlling thermal conductivities of flexible SUPE films (Fig. 3A). As the shearing speed increases, thermal conductivities of SUPE films along the shearing direction are notable improved, achieving 10.74 W m^{-1} K^{-1}at a shearing speed of 10 mm/s. A further increase of shearing speed induces a lower in-plane thermal conductivity (e.g., 9 W m^{-1} K^{-1} for 60 mm/s), which is consistent with the smaller crystallite or domain sizes resulted from the fast drying at a high shearing speed. The nonsheared polyethylene film has an in-plane thermal conductivity of 0.45 W m^{-1} K^{-1}. Figure 3B shows the stress versus strain curves of flexible SUPE films. With increasing the shearing speed from 5 to 60 mm/s, the yield strength of SUPE films increases from 11 to 17 MPa caused by the polymer chain alignment (*28*). The failure strengths increase from 19.5 to 24 MPa, and the failure strains of films increase from 720 to 950%, smaller than those with speed of 5, and 60 mm/s with strains of 920 and 950%, respectively, which are caused by highly aligned polymer chains. We next studied high-power electric insulation properties at high temperatures by using thermal conductive SUPE dielectric substrates (Fig. 3, C and D). As shown in Fig. 3C, the current ampacity of printed Cu hybrid electronics on SUPE clearly outperforms typical polymer dielectrics (i.e., Kapton). The current carrying capability of Cu features on SUPE is 25% larger than that of Kapton substrate. As the temperature is further raised to 100°C, the antenna performance of printed Cu electronics maintains as that of SUPE at 25°C (Fig. 3D). This indicates that, by replacing Kapton with SUPE, the electric insulation performance (high dielectric performance and high thermal conductivity) can eliminate the complex cooling system. The superior electric insulation performance of SUPE over other polymer dielectrics stems from its substantially increased dielectric performance and thermal conductivity at elevated temperatures.

The steady-state temperature distribution in the materials is modeled using finite element methods to compare thermal responses of Kapton and the SUPE used as electric insulator coating (see the Supplementary Materials). The simulation results are shown in Fig. 3 (E and F), in which the temperature in the bottom surface is fixed to 200°C, replicating the materials being in contact with copper conductor under the applied current density. Kapton poses isotropic thermal property with thermal conductivity of ~0.17 W m^{-1} K^{-1}, while the SUPE is anisotropic owing to the aligned polymer chains such that the conductivity in the *x* direction increases to ~11 W m^{-1} K^{-1}.

It can be seen in Fig. 3 (E and F) that because of the remarkable enhancement in directional thermal conductivity of SUPE, its steady-state internal temperature distribution is 42% lower than common

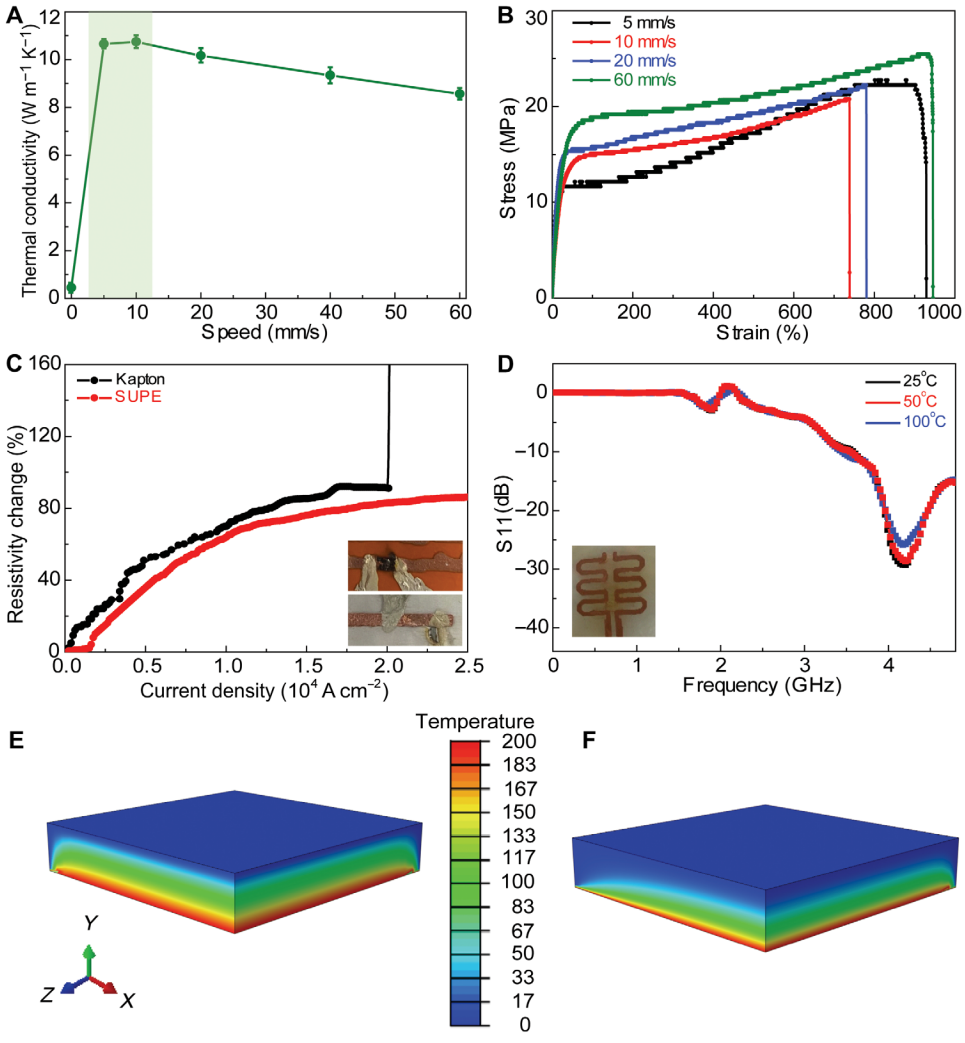

Fig. 3. Thermal and mechanical performance of SUPE films and its flexible hybrid electronics applications. (**A**) In-plane thermal conductivities versus shearing speed for SUPE films. (**B**) Tensile stress versus strain curves of shearing SUPE samples. (**C**) Resistivity change versus current density of printed copper features on flexible Kapton and SUPE film substrates. (**D**) Temperature dependence of the scattering parameter S11 for printed copper-SUPE antenna device within frequency ranging from 0 to 4.8 GHz. The inset is the antenna setup for printed copper features on SUPE substrate. Finite element simulations of the steady-state temperature distribution in (**E**) Kapton and (**F**) SUPE films. Photo credit: Zheng Li, University at Buffalo.

polymer insulation materials such as Kapton operating under the same environments. In these simulations, the average internal temperature is 52.5°C in SUPE and 89.9°C in Kapton. Such advanced thermal property of SUPE makes them a desired electric insulator material, while Kapton is expected to be overheated under high electrical current and even lose its electrical insulator functionality.

UHMWPE gel is also prepared in the presence of boron nitride (BN) nanosheets, shown in figs. S3 to S6. The BN nanosheets, a wide-bandgap (~6 eV) electric insulator material with thermal conductivity in the range from 300 to 2000 W m^{-1} K^{-1}, are prepared through liquid-phase exfoliation (Fig. 4A) (*29*, *30*). The thermal, mechanical, and dielectric performances are affected by the microstructures of SUPE/BN nanocomposite, the concentration and distribution of BN in SUPE matrix, and the interactions between BN nanosheets and polymer chains (*31*, *32*). The Fourier transform infrared spectroscopy of SUPE and SUPE/BN nanocomposites in Fig. 4B shows the transmittance intensity increase for the composite with 2 and 4 weight % (wt %) BN compared with SUPE, signifying the vibration strength changes of chemical groups in SUPE and SUPE/BN composites due to the BN and polymer chain interactions. The absorption peaks of 2917, 2848, 1467, and 722 cm^{-1} are attributed to methylene nonsymmetry stretch vibration, methylene symmetry stretch vibration, methylene nonsymmetry changing angle vibration, and methylene swing in plane vibration, respectively (*33*). The dielectric constant and Young's modulus versus BN concentrations in SUPE/BN are shown in Fig. 4C. The dielectric constant would increase from 4.12 to 4.42 with increasing BN concentration from 0 to 4 wt %. The stress-strain curves for SUPE/BN nanocomposites are shown in fig. S2, in which mechanical properties (modulus and strength) of SUPE/BN nanocomposites are increased with the addition of small quantities of exfoliated BN nanosheets (less than 6 wt %). The flexible SUPE film has a Young's modulus of 325 MPa and a failure strain of 870%, where the molecular chains inside readily move or relax under an applied load. The Young's modulus of SUPE/BN

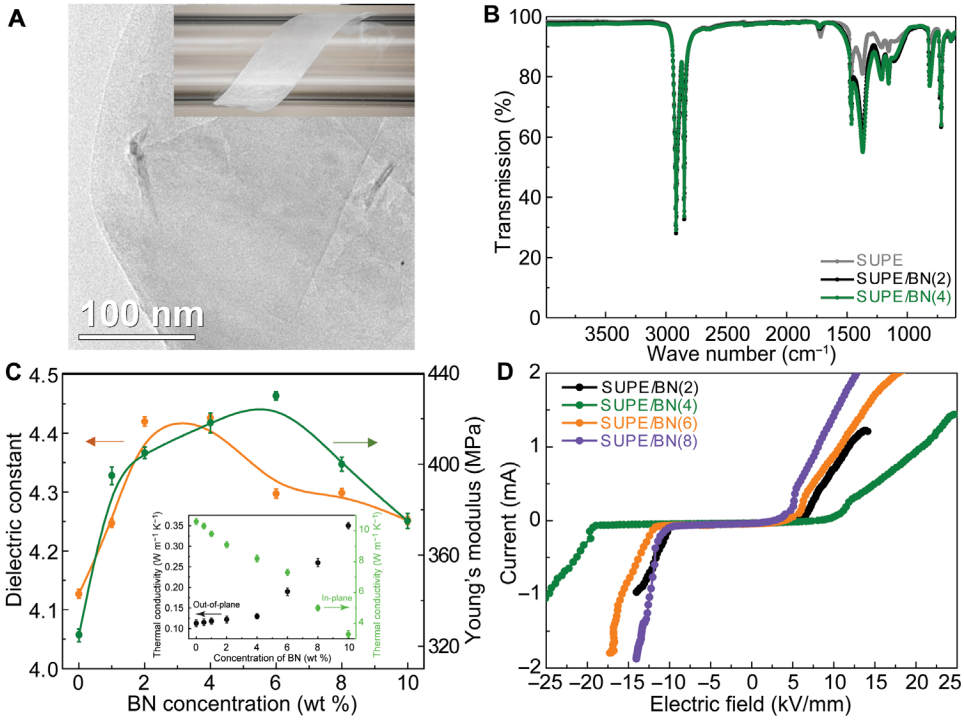

Fig. 4. Structural, dielectric, mechanical, thermal, and electrical properties of SUPE/BN composite films. (**A**) Transmission electron microscopy image of hexagonal BN (h-BN) nanosheets used in this work. The inset demonstrates the flexibility of transparent SUPE/BN composite film. (**B**) Fourier transform infrared spectroscopy spectra of SUPE and SUPE/BN composites with 2 and 4 wt % h-BN nanosheets. (**C**) Dielectric constant and Young's modulus versus BN concentration for SUPE/BN composites. The inset is the out-of-plane and in-plane thermal conductivity of SUPE/BN composites. (**D**) Dielectric strength of SUPE/BN composites with 2, 4, 6, and 8 wt % BN.

increases to 430 MPa when the BN concentration reaches 6 wt % and followed by a fall-off in modulus at a higher concentration of BN, which is attributed to the aggregation of BN nanosheets. Such behavior is also observed in some studies on polymer-nanotube and polymer-graphene composites (*19*, *33*). The thermal conductivities of SUPE/BN composites are also significantly enhanced in the thickness direction. Figure 4C also demonstrates the thermal conductivity versus the concentration of BN for SUPE/BN composites, where the SUPE/BN with 10 wt % BN is featured by the out-of-plane thermal conductivity of 0.35 W m^{-1} K^{-1}, approximately three times of out-of-plane thermal conductivity of SUPE. This could result from the thermal transport pathway composed of BN nanosheets in the SUPE/BN composite. Enhanced dielectric strength and high thermal conductivity are a long-term pursuit for the electrical insulation materials for the protection of high-power electronic applications. The dielectric strength of SUPE/BN is studied in Fig. 4D, which shows the superior electrical breakdown voltage of 11 kV/mm for SUPE/BN with 4 wt % BN. The composites with a higher or lower concentration of BN show the decreased electrical breakdown voltages, which are in accordance with the mechanical performance of SUPE/BN composites based on the Stark-Garton relationship (*34*).

In this study, solution SUPE shows not only significantly increased thermal conductivity but also high dielectric properties, particularly considering the nonpolar nature of polyethylene. The in-plane thermal conductivity of sheared flexible sheets reached 10.74 W m^{-1} K^{-1}, which is over 20 times higher than that of unstrained films. In addition, a high and robust dielectric constant across a broad temperature range and frequency is also found in flexible SUPE sheets. This improvement came from the synergistic collaboration of chain alignment, lattice strain, and compact connection arrangement, making it possible to obtain both high thermal conductivity and high dielectric properties. A holy grail energy-efficient polymer dielectric material demonstrated in this study has superior thermal conducting, mechanical and dielectric durability, and reliability across broad temperature and frequency ranges. These findings overcome two important hurdles in high-temperature electric insulation polymer materials by rationally designing the hierarchical structure through solution gel-shearing and lattice strains and by manufacturing lightweight, flexible polymers that can be shaped into intricate configurations for safe applications in high-power electronics and flexible advanced electric systems.

MATERIALS AND METHODS

Sheared UHMWPE film fabrication

UHMWPE powders (1 g) are mixed with 40 ml of decalin in a glass culture dish under convective thermal treatment at 170°C for 30 min. Then, the UHMWPE gel is drop-casted on a preheated glass substrate at 170°C, and the UHMWPE gel is rolled along a certain direction with different controlled speed by shear force. Last, the sheared UHMWPE film is formed and peeled off from the glass substrate at room temperature.

Sheared UHMWPE/hexagonal BN composite film fabrication

BN powders (1 g; diameter of 50 μm) are mixed with 300 ml of isopropanol to exfoliate monolayer or several-layer hexagonal BN (h-BN) nanosheets via ultrasonic sonication for 3 hours in ice bath with the parameters of 30-kHz cycle with 10-s pulse and 20-s stop.

The upper liquid is centrifuged after waiting for 12 hours and vacuum-dried for the next step. UHMWPE powders (0.2 g) are mixed with 10 ml of decalin in glass culture dish, which is then thermally treated at 170°C for 50 min. The UHMWPE/BN composites are prepared by a similar shearing method by adding different amounts of liquid-exfoliated BN nanosheet (0 to 10 wt %).

Morphology and structural characterization

The ultraviolet–visible (UV-vis) absorption and transmittance spectra are collected using an Agilent Cary 7000 UV-vis near-infrared spectrophotometer. A Raman microspectroscopy experiment is performed using a Renishaw inVia Raman microscope (Renishaw Inc., Hoffman Estates, IL), equipped with a Leica DM LM microscope (5×, 20×, and L50× objectives). Spectra are collected using a Renishaw diode laser [488 nm; irradiated area, ≈2 μm by 2 μm; grating, 1200 lines (l)/m]. The microstructure examination is performed on the Carl Zeiss AURIGA CrossBeam Focused Ion Beam Electron Microscope with an accelerating voltage of 200 kV and a point resolution of 0.19 nm. Thermal transitions are determined using a PerkinElmer (Shelton, CT) differential scanning calorimeter with a heating rate of 10°C/min. Thermal degradation is measured on a thermogravimetric analyzer (SDT Q600, TA Instruments, USA) under N_2 atmosphere. The crystal structure is characterized by x-ray diffraction (Rigaku Ultima IV instrument operating with a CuKα radiation).

Mechanical, dielectric, and thermal property

Tensile stress-strain curves for the sheared UHMWPE or UHMWPE/BN samples are performed with a Mark-10 universal testing machine. The thermal conductivities of both UHMWPE/BN and alignment UHMWPE are tested by Thermtest Hot Disk TPS 2200. The dielectric constant and dissipation factor are determined from an LCR meter with a frequency from 100 Hz to 2 MHz (Agilent E4980A). The dielectric testing area is defined as 1 cm by 1 cm using the shadow mask method.

Printable electronics for material reliability evaluations

The in-house copper ink is printed onto the dielectric substrates (*35*). To evaluate the effect of commercial Kapton and SUPE, the printed copper features with a length of 5 cm, a width of 2 mm, and a thickness of 10 μm are deposited on Kapton and SUPE substrates for the stability evaluation under different current density and temperatures.

SUPPLEMENTARY MATERIALS

Supplementary material for this article is available at https://science.org/doi/10.1126/sciadv.abi7410

REFERENCES AND NOTES

1. Q. Li, L. Chen, M. R. Gadinski, S. Zhang, G. Zhang, U. Li, E. Iagodkine, A. Haque, L.-Q. Chen, N. Jackson, Q. Wang, Flexible high-temperature dielectric materials from polymer nanocomposites. *Nature* **523**, 576–579 (2015).
2. W. J. Sarjeant, I. W. Clelland, R. A. Price, Capacitive components for power electronics. *Proc. IEEE* **89**, 846–855 (2001).
3. Q. Tan, P. Irwin, Y. Cao, Advanced dielectrics for capacitors. *IEEJ Trans. Fundam. Mater.* **126**, 1153–1159 (2006).
4. B. Chu, X. Zhou, K. Ren, B. Neese, M. Lin, Q. Wang, F. Bauer, Q. M. Zhang, A dielectric polymer with high electric energy density and fast discharge speed. *Science* **313**, 334–336 (2006).
5. C. Qian, A. M. Gheitaghy, J. Fan, H. Tang, B. Sun, H. Ye, G. Zhang, Thermal management on IGBT power electronic devices and modules. *IEEE Access* **6**, 12868–12884 (2018).
6. T.-L. Li, S. L.-C. Hsu, Enhanced thermal conductivity of polyimide films via a hybrid of micro- and nano-sized boron nitride. *J. Phys. Chem. B* **114**, 6825–6829 (2010).
7. M. J. Graf, S. K. Yip, J. A. Sauls, D. Rainer, Electronic thermal conductivity and the Wiedemann-Franz law for unconventional superconductors. *Phys. Rev. B Condens. Matter* **53**, 15147–15161 (1996).
8. A. Al-Gheilani, W. Rowe, Y. Li, K. L. Wong, Stress control methods on a high voltage insulator: A review. *Energy Procedia* **110**, 95–100 (2017).
9. T. R. Anthony, W. F. Banholzer, J. F. Fleischer, L. Wei, P. K. Kuo, R. L. Thomas, R. W. Pryor, Thermal diffusivity of isotopically enriched ^{12}C diamond. *Phys. Rev. B Condens. Matter* **42**, 1104–1111 (1990).
10. A. G. Gibson, D. Greig, M. Sahota, I. M. Ward, C. L. Choy, Thermal conductivity of ultrahigh-modulus polyethylene. *J. Polym. Sci. Polym. Lett. Ed.* **15**, 183–192 (1977).
11. S. Shen, A. Henry, J. Tong, R. Zheng, G. Chen, Polyethylene nanofibres with very high thermal conductivities. *Nat. Nanotechnol.* **5**, 251–255 (2010).
12. Y. Xu, D. Kraemer, B. Song, Z. Jiang, J. Zhou, J. Loomis, J. Wang, M. Li, H. Ghasemi, X. Huang, X. Li, G. Chen, Nanostructured polymer films with metal-like thermal conductivity. *Nat. Commun.* **10**, 1771 (2019).
13. C. L. Choy, W. H. Luk, F. C. Chen, Thermal conductivity of highly oriented polyethylene. *Polymer* **19**, 155–162 (1978).
14. H. Fujishiro, M. Ikebe, T. Kashima, A. Yamanaka, Drawing effect on thermal properties of high-strength polyethylene fibers. *Jpn. J. Appl. Phys.* **37**, 1994–1995 (1998).
15. J. Zhao, J. W. Jiang, N. Wei, Y. Zhang, T. Rabczuk, Thermal conductivity dependence on chain length in amorphous polymers. *J. Appl. Phys.* **113**, 184304 (2013).
16. C. L. Choy, Y. W. Wong, G. W. Yang, T. Kanamoto, Elastic modulus and thermal conductivity of ultradrawn polyethylene. *J Polym Sci B* **37**, 3359–3367 (1999).
17. J. I. Hong, P. Winberg, L. S. Schadler, R. W. Siegel, Dielectric properties of zinc oxide/low density polyethylene nanocomposites. *Mater. Lett.* **59**, 473–476 (2005).
18. Y. Huang, X. Wei, L. Liu, H. Yu, J. Yang, A novel pore-free strategy via interfacial effects in nanocomposites to produce polyethylene with ultra-low dielectric constants. *Mater. Lett.* **232**, 86–91 (2018).
19. Z. Zhang, S. Mogurampelly, S. Percec, Y. Hu, G. Fiorin, M. L. Klein, S. Ren, Mechanically strong polymer sheets from aligned ultrahigh-molecular-weight polyethylene nanocomposites. *J. Phys. Chem. Lett.* **9**, 2652–2658 (2018).
20. H. Hong, Y. H. Jung, J. S. Lee, C. Jeong, J. U. Kim, S. Lee, H. Ryu, H. Kim, Z. Ma, T. I. Kim, Anisotropic thermal conductive composite by the guided assembly of boron nitride nanosheets for flexible and stretchable electronics. *Adv. Funct. Mater.* **29**, 1902575 (2019).
21. Q. Song, W. Zhu, Y. Deng, F. Hai, Y. Wang, Z. Guo, Enhanced through-plane thermal conductivity and high electrical insulation of flexible composite films with aligned boron nitride for thermal interface material. *Compos. Part A Appl. Sci. Manuf.* **127**, 105654 (2019).
22. Z. Yu, Y. Bai, Y. Li, W. Wang, J. H. Wang, Preparation and performance of short carbon fiber and flake graphene reinforced polycarbonate composites: Effects of different toughener. *J. Mater. Sci. Chem. Eng.* **6**, 81–89 (2018).
23. H. L. Lee, O. H. Kwon, S. M. Ha, B. G. Kim, Y. S. Kim, J. C. Won, J. Kim, J. H. Choi, Y. Yoo, Thermal conductivity improvement of surface-enhanced polyetherimide (PEI) composites using polyimide-coated h-BN particles. *Phys. Chem. Chem. Phys.* **16**, 20041–20046 (2014).
24. C. L. Choy, K. W. Kwok, W. P. Leung, F. P. Lau, Thermal conductivity of poly(ether ether ketone) and its short-fiber composites. *J Polym Sci B* **32**, 1389–1397 (1994).
25. K. Uetani, K. Hatori, Thermal conductivity analysis and applications of nanocellulose materials. *Sci. Technol. Adv. Mater.* **18**, 877–892 (2017).
26. B. J. Worfolk, S. C. Andrews, S. Park, J. Reinspach, N. Liu, M. F. Toney, S. C. B. Mannsfeld, Z. Bao, Ultrahigh electrical conductivity in solution-sheared polymeric transparent films. *Proc. Natl. Acad. Sci. U.S.A.* **112**, 14138–14143 (2015).
27. G. Giri, E. Verploegen, S. C. Mannsfeld, S. Atahan-Evrenk, D. H. Kim, S. Y. Lee, H. A. Becerril, A. Aspuru-Guzik, M. F. Toney, Z. Bao, Tuning charge transport in solution-sheared organic semiconductors using lattice strain. *Nature* **480**, 504–508 (2011).
28. L. An, Z. Shao, J. N. Armstrong, Y. Huang, Y. Hu, Z. Li, D. Faghihi, S. Ren, Hierarchical structural engineering of ultrahigh-molecular-weight polyethylene. *ACS Appl. Mater. Interfaces* **12**, 50024–50032 (2020).
29. Q. Cai, D. Scullion, W. Gan, A. Falin, S. Zhang, K. Watanabe, T. Taniguchi, Y. Chen, E. J. G. Santos, L. H. Li, High thermal conductivity of high-quality monolayer boron nitride and its thermal expansion. *Sci. Adv.* **5**, eaav0129 (2019).
30. S. M. Kim, A. Hsu, M. H. Park, S. H. Chae, S. J. Yun, J. S. Lee, D. H. Cho, W. Fang, C. Lee, T. Palacios, M. Dresselhaus, K. K. Kim, Y. H. Lee, J. Kong, Synthesis of large-area multilayer hexagonal boron nitride for high material performance. *Nat. Commun.* **6**, 8662 (2015).
31. H. Shen, J. Guo, H. Wang, N. Zhao, J. Xu, Bioinspired modification of h-BN for high thermal conductive composite films with aligned structure. *ACS Appl. Mater. Interfaces* **7**, 5701–5708 (2015).
32. J. Wang, Y. Wu, Y. Xue, D. Liu, X. Wang, X. Hu, Y. Bando, W. Lei, Super-compatible functional boron nitride nanosheets/polymer films with excellent mechanical properties and ultra-high thermal conductivity for thermal management. *J. Mater. Chem. C* **6**, 1363–1369 (2018).

33. W. Pang, Z. Ni, G. Chen, G. Huang, H. Huang, Y. Zhao, Mechanical and thermal properties of graphene oxide/ultrahigh molecular weight polyethylene nanocomposites. *RSC Adv.* **5**, 63063–63072 (2015).
34. K. H. Stark, C. G. Garton, Electric strength of irradiated polythene. *Nature* **176**, 1225–1226 (1955).
35. Z. Li, S. Khuje, A. Chivate, Y. Huang, Y. Hu, L. An, Z. Shao, J. Wang, S. Chang, S. Ren, Printable copper sensor electronics for high temperature. *ACS Appl. Electron. Mater.* **2**, 1867–1873 (2020).

Acknowledgments
Funding: Financial support at University at Buffalo (S.R.) was provided by the U.S. Army Research Laboratory under award W911NF-20-2-0016. **Author contributions:** Z.L. and S.R. designed the experiment. Z.L. fabricated the samples and analyzed the data. L.A. helped with the mechanical measurements. J.T. and D.F. conducted the finite element simulations. S.K. prepared printed electronics devices. Y. Hu helped with the test of dielectric strength. Y. Huang carried out the TGA measurement. D.P. helped with the test of thermal conductivity. J.Y. carried out the high-frequency dielectric measurement. All authors analyzed and discussed the results and commented on the manuscript. **Competing interests:** The authors declare that they have no competing interests. **Data and materials availability:** All data needed to evaluate the conclusions in the paper are present in the paper and/or the Supplementary Materials.

Submitted 27 March 2021
Accepted 5 August 2021
Published 29 September 2021
10.1126/sciadv.abi7410

Citation: Z. Li, L. An, S. Khuje, J. Tan, Y. Hu, Y. Huang, D. Petit, D. Faghihi, J. Yu, S. Ren, Solution-shearing of dielectric polymer with high thermal conductivity and electric insulation. *Sci. Adv.* **7**, eabi7410 (2021).